Geochemistry, Geophysics, Geosystems®

RESEARCH ARTICLE
10.1029/2025GC012272

Sound Velocities of Basaltic Glass at Earth's Deep-Mantle Pressures

Xiaowan Su[1], Jin Liu[2,3], Yongsheng Zhou[1], Jun Hu[2], Mathieu Roskosz[4], and Jung-Fu Lin[3]

[1]State Key Laboratory of Earthquake Dynamics and Forecasting, Institute of Geology, China Earthquake Administration, Beijing, China, [2]State Key Laboratory of Metastable Materials Science and Technology, Center for High Pressure Science, Yanshan University, Qinhuangdao, China, [3]Department of Geological Sciences, Jackson School of Geosciences, The University of Texas at Austin, Austin, TX, USA, [4]IMPMC-UMR CNRS 7590, Sorbonne Universités, UPMC, IRD, MNHN, Muséum National d'Histoire Naturelle, Paris, France

Key Points:

- The V_P and V_S of a basaltic glass were measured up to 63 GPa using Brillouin and impulsive-stimulated light scattering methods
- The addition of Al_2O_3 can enhance the V_S and V_P of the basaltic glass, whereas FeO and CaO substitutions decrease its velocities
- Basaltic melts with significant amounts of FeO and $A_{l2}O_3$ may also become less buoyant at the mid-lower mantle depth of 1,500 km

Supporting Information:

Supporting Information may be found in the online version of this article.

Correspondence to:

J. Liu and J.-F. Lin,
jinliu@ysu.edu.cn;
afu@jsg.utexas.edu

Citation:

Su, X., Liu, J., Zhou, Y., Hu, J., Roskosz, M., & Lin, J.-F. (2025). Sound velocities of basaltic glass at Earth's deep-mantle pressures. *Geochemistry, Geophysics, Geosystems*, *26*, e2025GC012272. https://doi.org/10.1029/2025GC012272

Received 5 MAR 2025
Accepted 16 JUL 2025

Author Contributions:

Data curation: Jin Liu
Funding acquisition: Xiaowan Su, Jin Liu, Yongsheng Zhou, Jung-Fu Lin
Writing – original draft: Xiaowan Su
Writing – review & editing: Xiaowan Su, Jin Liu, Yongsheng Zhou, Jun Hu, Mathieu Roskosz, Jung-Fu Lin

Abstract The elasticity of compressed silicate melts is essential to decipher seismic properties and dynamic evolution of deep mantle magmas. Here, we report the compressional (V_P) and shear (V_S) wave velocities of a basaltic glass ($Na_{0.036}Ca_{0.220}Mg_{0.493}Fe_{0.115}Al_{0.307}Ti_{0.012}K_{0.002}Si_{0.834}O_3$) up to 63 GPa at 300 K using Brillouin and impulsive stimulated light scattering spectroscopies coupled with diamond anvil cells. The V_P and V_S data from 2.4 to 62.8 GPa exhibit convex upward trend, but the pressure-dependent velocity slopes become flatter at around 38 ± 3 GPa. The V_P and V_S values increase from 6.86 ± 0.03 to 11.62 ± 0.20 km/s and from 3.70 ± 0.03 to 5.28 ± 0.07 km/s, respectively. These velocity behaviors are likely associated with the 4- to 6-fold silicon coordination number increase. Comparison with literature data on $MgSiO_3$ glass, silicate, and pyrolitic glasses at high pressure suggests that the addition of Al_2O_3 can enhance the V_S and V_P of the basaltic glass, whereas FeO and CaO substitutions decrease its velocities. Using our results as an analog for basaltic melts, which can incorporate significant amounts of Al_2O_3 and FeO, the countercationic effects of Al_2O_3 and FeO on velocities and density of the basaltic melt could make it less visible seismically at the mid-lower mantle depths of ~1,500 km.

Plain Language Summary Basaltic magmas can be produced through partial melting of the mantle peridotite or remnants of the early magma ocean. Their presence in the Earth's mantle can be revealed by seismic wave velocity variations, and is important to our understanding of the planet's physical and chemical evolution. Laboratory measurements of the acoustic wave velocities of basaltic glasses could be used as analogs to tackle this outstanding issue. Here, we carried out acoustic wave velocity measurements on a representative basaltic glass up to mid-lower mantle pressure of 63 GPa (corresponding to 1,500 km depth). The basaltic glass exhibits pressure-enhanced velocity behaviors with a flatter slope above 38 ± 3 GPa. These velocity-pressure curves are interpreted as a result of compression-induced silicon coordination increase from 4- to 6-fold in average. Basaltic melts in Earth's midlower mantle are expected to contain significant amount of Al_2O_3 and FeO, which could have countereffects on the velocity and density, making it less visible seismically.

1. Introduction

Knowledge of the local atomic structures and physical properties of deep mantle magma at high pressure-temperature (P-T) conditions is essential to understanding Earth's early dynamic processes related to melting, element partitioning, and thermal and chemical evolution of the planet (Labrosse et al., 2007; Ohtani et al., 1995). Iron-rich basaltic melts have been considered as possible remnants of deep-seated magmas in the lower mantle (e.g., Du et al., 2019; Labrosse et al., 2007). Previous studies revealed that the fate of basaltic melts in the deep Earth is strongly influenced by their densities, which are affected by local structures and compositions at depths (Clark et al., 2016; Du et al., 2019; Liu & Lin, 2014; Lobanov et al., 2022; Ohtani & Maeda, 2001; Petitgirard et al., 2015, 2017). To date, a number of experiments and calculations have been conducted to investigate the elasticity (e.g., sound velocities and density (ρ)) and local structures of basaltic melts under pressure, including Brillouin light scattering (BLS) and impulsive-stimulated light scattering (ISLS) spectroscopies (Liu & Lin, 2014; Mashino et al., 2022; Murakami and Bass, 2010, 2011; Sanchez-Valle & Bass, 2010; Sun et al., 2022; Zha et al., 1994), X-ray Raman and infrared spectroscopies (Hemley et al., 1986; Lee et al., 2008, 2019; Williams & Jeanloz, 1988), angle-dispersive and energy-dispersive X-ray diffraction spectra (Kono et al., 2018; Prescher

et al., 2017), and first-principles and molecular dynamics simulations (Ghosh et al., 2014; Shimoda & Okuno, 2006). Notably, accurate acoustic wave velocity measurements have played a key role in relating the elasticity of basaltic glasses/melts to local atomistic structures, compositions, and seismic models in the Earth's mantle (Huang et al., 2022; Mashino et al., 2022; Murakami & Bass, 2010, 2011; Ohira et al., 2016; Saha et al., 2023; Trubowitz et al., 2024).

Basaltic glasses have been conventionally studied as analogs for basaltic melts under high pressure, taking into account that glasses and melts share the similarities in their local atomic structures and that glasses can be more readily used for high pressure experiments (Elliott, 1992; Hennet et al., 2007; Price et al., 1988; Susman et al., 1990). Thus far, the acoustic wave velocity measurements of silicate glasses have been extensively investigated at pressures below 25 GPa (Aoki et al., 2020; Clark et al., 2016; Gu et al., 2021; Liu & Lin, 2014; Murakami & Bass, 2010; Sakamaki et al., 2014; Sanchez-Valle & Bass, 2010; Xu et al., 2018). Above 25 GPa which corresponds to the topmost lower-mantle pressures, sound velocity results of silicate glasses such as SiO_2 glass (Sun et al., 2022; Zha et al., 1994), $MgSiO_3$ glass (Murakami & Bass, 2011; Sanchez-Valle & Bass, 2010), Fe^{2+}-bearing $MgSiO_3$ glass (Mashino et al., 2022), (Fe^{2+} and Al)-bearing silicate glass (Saha et al., 2023), basaltic glass (Liu & Lin, 2014; Trubowitz et al., 2024), and pyrolitic glass (Huang et al., 2022) are only limited in a number of reports, which mainly focused on Vs data. In the multi-component basaltic glasses, previous studies suggested that the type and content of network modifier cations (e.g., Mg, Ca, Fe, Al, K, and Na) could change the elastic properties of silicate glasses (Aoki et al., 2020; Liu & Lin, 2014; Sun et al., 2022). For instance, the addition of 12 mol.% FeO decreases the V_S of $MgSiO_3$ glass up to 5.5% (Mashino et al., 2022). However, simultaneous V_P and V_S profiles of basaltic glass with a relevant composition at lower-mantle pressures remain largely unconstrained. This drawback is largely due to the technical difficulty of measuring high-pressure V_P because its signals were blocked by diamond windows in DACs in BLS experiments, which remain the main method of the high-pressure V_S studies (Mashino et al., 2022; Murakami & Bass, 2011). We should note that the V_S values of glasses at high pressure are more relevant to the shear modulus (μ) and ρ ($V_S = (\mu/\rho)^{1/2}$), whereas V_P data of silicate glasses at high pressure are more representative of the bulk modulus (k) ($V_P = ((4/3\mu + k)/\rho)^{1/2}$). However, V_P is rather challenging to obtain at high pressure. Hence, combined measurements of both V_P and V_S values of basaltic glasses with relevant compositions at lower-mantle pressure are needed to significantly advance our knowledge in the field.

In this study, the V_P and V_S of a tholeiite basaltic glass were measured using BLS and ISLS spectroscopies in DACs up to 63 GPa at ambient temperature (J. Yang et al., 2015). The use of ISLS technique allowed us to measure the V_P of the basaltic glass at the unprecedented pressure range. We then derived the Poisson's ratio (ν) of the basaltic glass directly from the measured V_S and V_P values as pressure rises. These results are applied to correlate with the elastic properties of the basaltic glass with pressure-induced structural changes. Moreover, compared with literature data, the effects of composition on elastic properties of the basaltic glass are evaluated. These results are applied to discuss the behavior of the basaltic melts at high pressure to provide insights into the dynamics and evolution of deep magma in the mantle.

2. Methods

2.1. Synthesis of Tholeiite Basaltic Glass

The tholeiite basaltic glass was synthesized in a vertical tube furnace at the University of Lille (France) (see Dauphas et al. (2014) for more details of the sample synthesis and characterizations). Briefly, reagent-grade oxides of SiO_2, $CaCO_3$, Al_2O_3, MgO, K_2CO_3, Na_2CO_3, TiO_2, and Fe_2O_3 were mechanically mixed to serve as starting materials. The mixtures were pressed into a cylindrical sample of ∼2 mm in thickness and ∼2 mm in diameter. The cylindrical sample was enclosed in a Pt wire loop and heated for 1 hr in a CO/CO_2 gas-mixing furnace at 1873 K and Log (fO_2) ≈ −8 (IW + 0.3). Then, the molten sample was rapidly quenched. The composition and homogeneity of the quenched glass were confirmed by electron microprobe analysis, resulting in $Na_{0.036}Ca_{0.220}Mg_{0.493}Fe_{0.115}Al_{0.307}Ti_{0.012}K_{0.002}Si_{0.834}O_3$ with $Fe^{3+}/Fe_{total} < 0.02$. The density of tholeiitic basalt glass is 2.78 g/cm^3 at ambient conditions. Additionally, this sample was used in a previous study using nuclear resonant inelastic X-ray scattering on the force constants of iron bonds at high pressure (Liu et al., 2017). The synthesized tholeiite basaltic glass was used for the BLS and ISLS experiments.

2.2. High-Pressure Brillouin Light Scattering Measurements

BLS experiments were performed up to 63 GPa at an interval of 2–5 GPa in the Mineral Physics Laboratory of the University of Texas at Austin (Fu et al., 2017, 2018; J. Yang et al., 2015). A piece of the glass sample was polished on double sides using 3M diamond films to approximate 17 μm in thickness. Subsequently, it was cut into a small platelet with ~70 μm in diameter. A rhenium (Re) gasket was pre-indented to a thickness of ~30 μm using a short symmetric DAC with 300 μm culets. A 160 μm diameter hole was drilled in the pre-indented gasket. Neon was loaded as a pressure-transmitting medium, and two ruby spheres were used as pressure gauges. Ruby fluorescence spectra were measured before and after each BLS measurement to evaluate pressure uncertainties (Mao et al., 1986).

The BLS system consists of a Coherent Verdi V2 laser with a wavelength of 532 nm, a JRS Fabry-Perot interferometer and a Count-10B avalanche photodiode detector with a low dark count rate of 5 c/s. The Coherent Verdi V2 laser generates an incident laser beam interacting with the sample, and it would lead to a frequency shift of the scattered radiation. The frequency shift was collected by the JRS Fabry-Perot interferometer (Fu et al., 2017; Liu & Lin, 2014; J. Yang et al., 2014, 2016). Time for data collection for each BLS spectra was 1–2 hr below 30 GPa and 2–3 hr at higher pressure. Subsequently, these BLS spectra were analyzed through OriginPro 9.1 software. The strong V_P and V_S peaks with high signal-to-noise ratios were observed below 32 GPa, while only the V_S peaks of the sample were observed at pressures greater than 32 GPa. The V_P peaks of the glass sample above 32 GPa were overlapped by the diamond anvil's transverse acoustic modes (Figure S1 in Supporting Information S1). The acoustic velocities (V_P and V_S) were directly calculated through Gaussian function as follows:

$$V_{P,S} = \frac{\Delta\nu_B \lambda_0}{2\sin(\theta/2)} \quad (1)$$

where $V_{P,S}$ is the measured acoustic velocities, $\Delta\nu_B$ is the measured Brillouin frequency shift, λ_0 is the laser wavelength of 532 nm, and θ is the scattering angle of 48.1°.

2.3. High-Pressure Impulsive Stimulated Light Scattering Measurements

High-pressure ISLS measurements were also performed on the glass sample in the DAC between 24 and 63 GPa at UT Austin. The ISLS system is known as a pump-and-probe spectroscopy. The wavelengths of the pump laser and the probe laser are 1,064 and 532 nm, respectively. The pulse width of the two lasers is 15 picoseconds, together with a repetition rate of 200,000 Hz. The pump laser is first divided into two beams, which are then recombined to a diameter of 20 μm at the sample position. The crossing angle is set up to 20.3°, which is regularly calibrated using silica glass and distilled water (Fu et al., 2017; J. Yang et al., 2016). The probe laser was delayed up to 20 ns by an Aerotech linear stage. A photodiode detector was used to collect the diffracted ISLS signals of the sample. Based on the Burg method, ISLS signals are further Fourier-transformed from the time domain to the frequency domain using MATLAB and OriginLab Pro 9.1 program (Fu et al., 2017; J. Yang et al., 2016). Subsequently, the frequency-domain power spectra were employed to calculate the V_P values of the basaltic glass (Figure S2 in Supporting Information S1). Each ISLS spectrum was collected up to ~4 hr. Before and after each ISLS measurement, the pressure and its uncertainty were double checked through ruby fluorescence spectra.

3. Results and Discussion

3.1. Sound Velocities of the Basaltic Glass at High Pressures

Analyses of the BLS spectra reveal the V_S and V_P of the basaltic glass up to 62.8 and 31.4 GPa, respectively. Above 31.4 GPa, the V_P was masked out by the V_S of diamond anvils. ISLS results also show the V_P of the glass at 23.7–62.8 GPa (Figure 1 and Table S1 in Supporting Information S1), which are consistent with those from BLS analyses (Table S1 in Supporting Information S1 and Figure 1b). This affirms the reliability of the data from both techniques for complementary high-pressure velocity measurements and further modeling of elastic parameters (Fu et al., 2017; J. Yang et al., 2016).

At 0–2.4 GPa, the V_S and V_P values of the basaltic glass abnormally decrease from 3.82 ± 0.03 and 6.92 ± 0.03 km/s at ambient conditions to 3.70 ± 0.03 and 6.86 ± 0.03 km/s at 2.4 GPa, respectively (Figure 1). This type of the pressure-induced velocity reduction has also been observed in silica and silicate glasses (Liu &

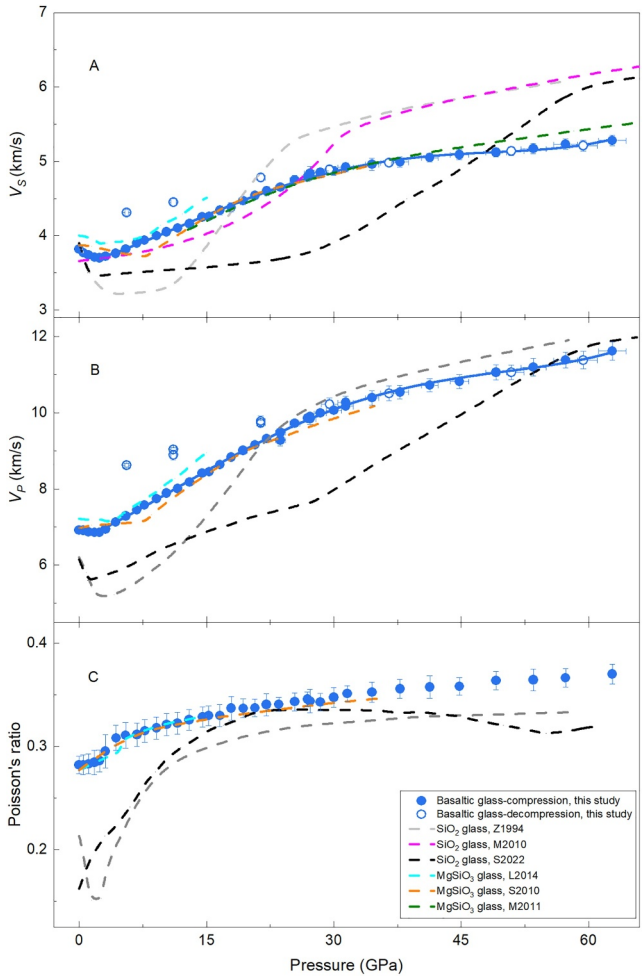

Figure 1. Elastic properties of the basaltic glass as a function of pressure. (a) Shear wave velocity (V_S). (b) Compressional wave velocity (V_P). (c) Poisson's ratio (ν). Solid and open symbols: our basaltic glass in compression and decompression, respectively; blue solid curves: fits to experimental data, this study; gray, magenta and black dashed curves: SiO_2 glass by Zha et al. (1994), Murakami and Bass (2010), and Sun et al. (2022), respectively; cyan, orange, and olive dashed curves: $MgSiO_3$ glass by Liu and Lin (2014), Sanchez-Valle and Bass (2010), and Murakami and Bass (2011), respectively. Vertical ticks represent errors ($\pm 1\sigma$) calculated using standard error propagations.

Lin, 2014; Murakami & Bass, 2010; Sun et al., 2022; Zha et al., 1994). This velocity softening behavior has been proposed to be closely related to collapse of topological voids through reductions in the ring sizes and Si-O-Si angles (Hemley et al., 1986; Sakamaki et al., 2014; Stixrude & Bukowinski, 1991). Kono et al. (2022) further showed that the fifth neighbor silicon atom located in the second shell collapsed onto the first shell, resulting in the disappearance of the large void structure in SiO_2 glass.

From 2.4 to 62.8 GPa, the V_S–P and V_P–P profiles of the basaltic glass exhibit a convex upward trend with a gentle gradient with increasing pressure (Figure 1). In this pressure range, the V_S and V_P velocities increase from 3.70 ± 0.03 to 5.28 ± 0.07 km/s and from 6.86 ± 0.03 to 11.62 ± 0.20 km/s, respectively. The V_S and V_P gradients appear to become flatter above 38 ± 3 GPa. This signals pressure-dependent effect on the velocities which are related to underlying structural changes of multiple cationic oxides (MgO, FeO, CaO, SiO_2, and Al_2O_3). To further evaluate the velocity evolutions, the V_S and V_P data at 2.4–62.8 GPa were fitted using fourth order polynomial functions, yielding an adjusted $R^2 = 0.9986$ for V_S and an adjusted $R^2 = 0.9990$ for V_P (Figures 1a and 1b). The R^2 value for our V_S–P profile is quite satisfactory with the previous results of SiO_2 glass with $R^2 = 0.9964$ (Murakami & Bass, 2010), $MgSiO_3$ glass with $R^2 = 0.9985$ (Murakami & Bass, 2011), $Fe_{0.12}Mg_{0.88}SiO_3$ glass with $R^2 = 0.9972$ (Mashino et al., 2022), $Mg_{0.92}Fe_{0.07}Si_{0.94}Al_{0.09}O_3$ glass with $R^2 = 0.9989$ (Saha et al., 2023), Al_2O_3-SiO_2 glass with $R^2 > 0.99$ (Ohira et al., 2016), basaltic glass with $R^2 > 0.99$ (Trubowitz et al., 2024), and pyrolitic glass with $R^2 = 0.9950$ (Huang et al., 2022). Notably, the pressure derivatives of the fitted curves, dV_S/dP and dV_P/dP, decrease gradually with increasing pressure from 10.3 to 37.8 GPa. At greater pressure, these derivatives remain nearly constant, and reach 0.01 and 0.04 km/s per GPa for dV_S/dP and dV_P/dP, respectively. The transition pressure at 38 ± 3 GPa is largely consistent with the pressure identified from molecular dynamics simulations for basaltic melts, where the increase in Si-O coordination starts to decelerate and flatten prior to reaching an average sixfold state (Bajgain et al., 2015; Dufils et al., 2017; Feng et al., 2021; Majumdar et al., 2020). Previous studies on glasses also indicate that the second derivative of the fitted function with respect to pressure (d^2V_S/dP^2) can also be a strong indicator of the structural changes in the Si-O coordination number from sixfold to a higher coordination state (Huang et al., 2022; Mashino et al., 2022; Murakami & Bass, 2010, 2011; Ohira et al., 2016; Saha et al., 2023; Trubowitz et al., 2024). The absence of such d^2V_S/dP^2 maximum value in our velocity data suggests that our basaltic glass might undergo a gradual transition in the silicon coordination number from four to six at 2.4–62.8 GPa.

Upon decompression from 62.8 to 31.4 GPa, the V_S and V_P values of the basaltic glass were consistent with those measured during compression. This indicates that the pressure-induced structural changes are reversible for the basaltic glass at 31.4–62.8 GPa. On the contrary, on further decompression from 31.4 GPa to ambient conditions, a large irreversible behavior of the V_S and V_P was observed for our basaltic glass. For instance, the V_S and V_P differences between the compression and decompression paths at 5.6 GPa could reach as large as 0.49 and 1.40 km/s, respectively (Figures 1a and 1b). A similar irreversible trend has been observed for SiO_2 and $MgSiO_3$ glasses during decompression (Sanchez-Valle & Bass, 2010; Sun et al., 2022; Zha et al., 1994). Zha et al. (1994) and Sun et al. (2022) suggested the irreversible compaction behavior of SiO_2 glass during decompression is likely due to the presence of the interpolyhedra connectivity dominated by edge sharing. Meanwhile, Sanchez-Valle and Bass (2010) reported that the irreversible structural changes in the intermediate-range order is the dominant reason for the irreversible densification of $MgSiO_3$ glass. Above all, the irreversibility exhibited by basaltic glass may stem from the retention of high-pressure structural features within its intermediate-range order when subjected to decompression to ambient conditions.

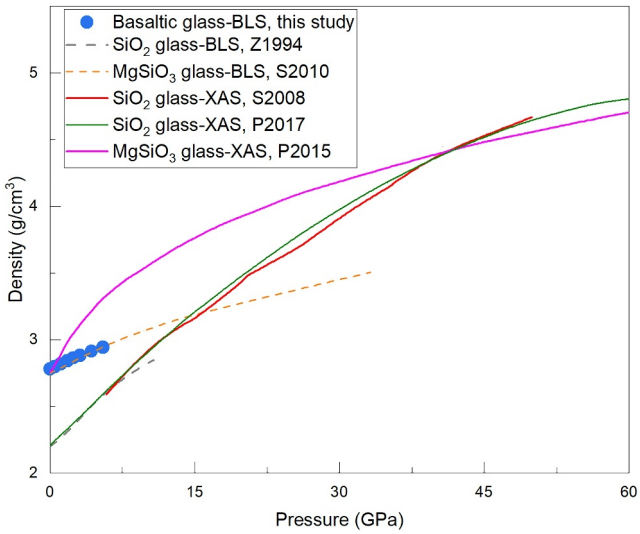

Figure 2. Calculated density of the basaltic glass as a function of pressure. Blue circles: our basaltic glass; magenta line: $MgSiO_3$ glass measured using X-ray absorption method, Petitgirard et al. (2015); red and olive curves: SiO_2 glass reported by Sato and Funamori (2008) and Petitgirard et al. (2017), respectively, using X-ray absorption method; gray curve: SiO_2 glass calculated from Brillouin data, Zha et al. (1994); orange line: $MgSiO_3$ glass calculated from Brillouin data, Sanchez-Valle and Bass (2010).

3.2. Poisson's Ratio of the Basaltic Glass at High Pressures

The ν value can be obtained directly from the measured V_S and V_P values by the following equation:

$$\nu = \frac{1}{2}\frac{(V_P/V_S)^2 - 2}{(V_P/V_S)^2 - 1} \quad (2)$$

The ν of our basaltic glass sample with increasing pressure is shown in Figure 1c. This pressure evolution could be broadly divided into the two regions based on its pressure dependence. Our basaltic glass sample's ν value increases monotonically with pressure approximately from 0.28 at 1 bar to 0.35 at 31.4 GPa. This trend is similar in the SiO_2 and $MgSiO_3$ glasses, resulting from the silicon coordination changes from fourfold to sixfold (Benmore et al., 2010; Lee et al., 2008; Meade et al., 1992; Sanchez-Valle & Bass, 2010; Sato & Funamori, 2010; Shim & Catalli, 2009; Sun et al., 2022; Zha et al., 1994). By contrast, the ν value of the basaltic glass is nearly pressure-independent above 31.4 GPa. Similarly, SiO_2 glass also exhibits a pressure-independent trend above 23 GPa (Lin et al., 2007; Zha et al., 1994).

3.3. Density of the Basaltic Glass Below 5.6 GPa

Sound velocity data for amorphous glasses can be useful to calculate their density at high pressure (Zha et al., 1994). However, this method would fail when the irreversible behavior of the sound velocity of amorphous glass is present (Petitgirard et al., 2015; Sanchez-Valle & Bass, 2010). In particular, the calculated and measured density values for $MgSiO_3$ glass are different at 0–35 GPa, ascribed to its irreversible behavior in this pressure region (Figure 2). The reason is that only elastic, but not the configurational contributions to the compressibility, are probed by Brillouin scattering, while both the elastic and configurational contributions to the compressibility are probed by the X-ray absorption method. Notably, our basaltic glass sample shows different V_S and V_P values at 5.6 GPa between compression and decompression (Figures 1a and 1b). It means that the pressure-induced structural changes are inelastic and irreversible for the basaltic glass above 5.6 GPa. As such, the sound velocity collected in this study is unrelaxed above 5.6 GPa and cannot be used for the density calculation using the following relationships:

$$\rho_P - \rho_0 = \int_{P_0}^{P} \gamma dP / V_B^2 \quad (3)$$

$$V_B^2 = V_P^2 - 4V_S^2/3 \quad (4)$$

where ρ_P is the density of the basaltic glass at high pressure, ρ_0 is the density of the basaltic glass of 2.78 g/cm^3 at ambient conditions in this work, γ is the specific heat ratio of 1.0, and V_B is the bulk sound velocity.

Assuming that the compression of the basaltic glass is elastic and reversible below 5.6 GPa, the density of our basaltic glass sample was calculated up to 5.6 GPa using Equations 3 and 4. The calculated density values of our basaltic glass sample are compared with previous SiO_2 and $MgSiO_3$ glasses (Figure 2). The density values of our basaltic glass increase with increasing pressure at 0–5.6 GPa and reach 2.94 g/cm^3 at 5.6 GPa. Further, the calculated density values of SiO_2 glass are in good agreement with those measured by using the X-ray absorption method below 10 GPa, where SiO_2 glass exhibits a reversible compression behavior (Petitgirard et al., 2017; Sato & Funamori, 2008; Zha et al., 1994).

3.4. Compositional Dependence of Sound Wave Velocities

Between 2.4 and 62.8 GPa, the V_S–P and V_P–P profiles of our basaltic glass exhibit convex upward trend with a gentle gradient, which is also observed in previous reported $MgSiO_3$ glass (Murakami & Bass, 2010), Al_2O_3-SiO_2 glass (Ohira et al., 2016), $Mg_{0.88}Fe_{0.12}SiO_3$ glass (Mashino et al., 2022), $Mg_{0.92}Fe_{0.07}Si_{0.94}Al_{0.09}O_3$ glass (Saha

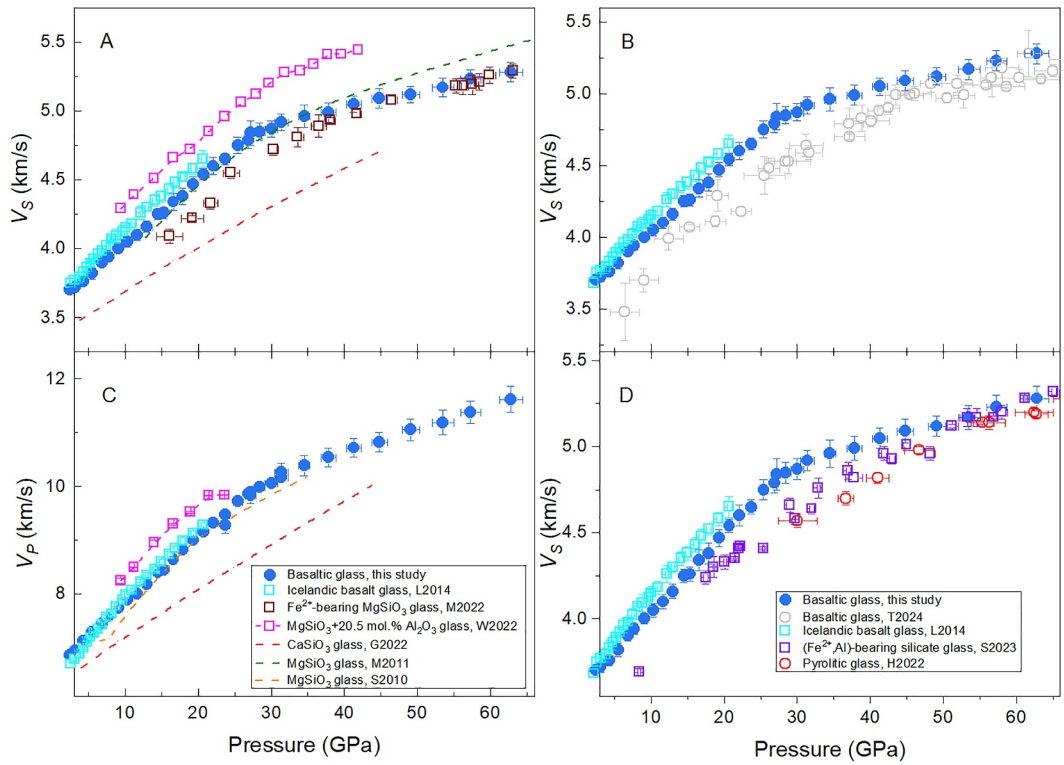

Figure 3. Comparison of the V_S (a, b, d) and V_P (c) values for various silicate glasses at high pressure. Solid circles: our basaltic glass; cyan squares: Icelandic basalt glass by Liu and Lin (2014); wine squares: $Mg_{0.88}Fe_{0.12}SiO_3$ glass by Mashino et al. (2022); magenta squares: $MgSiO_3$·20.5 mol.% Al_2O_3 glass by Wei et al. (2022); purple squares: (Fe^{2+} and Al)-bearing silicate glass by Saha et al. (2023); gray circles: basaltic glass by Trubowitz et al. (2024); red circles: pyrolitic glass by Huang et al. (2022); red curve: $CaSiO_3$ glass by Geballe et al. (2022); olive curve: $MgSiO_3$ glass by Murakami and Bass (2011); and orange curve: $MgSiO_3$ glass by Sanchez-Valle and Bass (2010).

et al., 2023), basaltic glass (Trubowitz et al., 2024), and pyrolytic glass (Huang et al., 2022). The increase in the coordination number of silicon from four to six might be the dominant compression mechanism in this pressure region. To evaluate the compositional effect on sound velocities, the data are compared with literature data at high pressure (Huang et al., 2022; Mashino et al., 2022; Murakami & Bass, 2010; Ohira et al., 2016; Saha et al., 2023; Trubowitz et al., 2024). As shown in Figures 3a and 3c, the V_S and V_P values of $MgSiO_3$·20.5 mol.% Al_2O_3 glass are ~6.8% and ~5.5% greater than that of $MgSiO_3$ at 10–20 GPa (Ohira et al., 2016). This indicates that the sound velocities of $MgSiO_3$ glass are increased by the addition of Al_2O_3 component. In contrast, both $CaSiO_3$ and Fe-bearing $MgSiO_3$ glasses display lower V_S–P and V_P–P profiles than those of $MgSiO_3$ glass below 40 GPa, which could be explained by their higher density caused by the addition of heavy FeO and CaO components (Geballe et al., 2022; Mashino et al., 2022). These observations indicate that both V_S and V_P values of $MgSiO_3$ glass are increased by the addition of Al_2O_3 component but are reduced by the presence of FeO and CaO components. The sound velocities of the chemically complex silicate glasses could be simply regarded as the combined effect of FeO, CaO and Al_2O_3 components on the $MgSiO_3$ glass. Our basaltic glass contains ~1 mol.% smaller FeO, ~1 mol.% smaller Al_2O_3, and ~3 mol.% smaller CaO than that of the Icelandic basalt glass, which shows a ~2.0% higher V_S than our basaltic glass (Figure 3b and Table S2 in Supporting Information S1) (Liu & Lin, 2014). This means that the total reduction of V_S caused by the ~1 mol.% FeO and ~3 mol.% CaO is still less than the V_S increment caused by ~1 mol.% Al_2O_3. Meanwhile, the V_S values of our basaltic glass are ~3.3% higher than that of another basaltic glass reported by Trubowitz et al. (2024) at 2.4–62.8 GPa (Figure 3b). As shown in Table S2 in Supporting Information S1, the FeO content in those two basaltic glasses is comparable (~6 mol.%), but our basaltic glass contains 2 mol.% smaller Al_2O_3 and 3 mol.% smaller CaO. It is thus conceivable that the V_S increment caused by 2 mol.% Al_2O_3 is higher than the V_S reduction induced by 3 mol.% CaO in basaltic glasses. Compared to the (Fe^{2+} and Al)-silicate glass, the pyrolitic glass exhibits a ~2.8% smaller V_S, most likely because it contains ~2 mol.% FeO and ~2 mol.% CaO (Figure 3d and Table S2 in Supporting Information S1) (Huang et al., 2022; Saha et al., 2023).

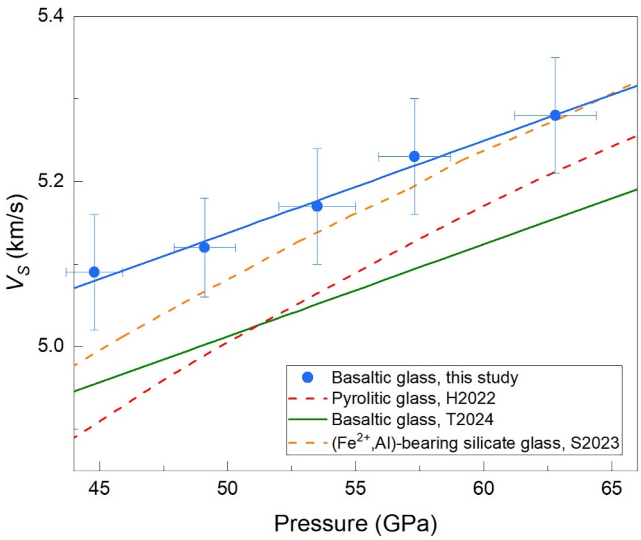

Figure 4. The V_S of the multi-component silicate glasses as a function of pressure. The effect of Al_2O_3 (a) and FeO (b) contents on the reduction of the inflection pressure in selected silicate glasses. Blue circles: our basaltic glass; blue curve: fits to experimental data in this study; olive curve: basaltic glass by Trubowitz et al. (2024); orange curve: (Fe^{2+} and Al)-bearing silicate glass by Saha et al. (2023); and red curve: pyrolitic glass by Huang et al. (2022).

The comparison of literature data also reveals that sound velocities of compressed glasses can be influenced by the synthesis methods of starting samples and experimental environments. As shown in Figure 1, the sound velocity of SiO_2 glass reported by Sun et al. (2022) was significantly different from that reported by Zha et al. (1994) and Murakami and Bass (2010). The differences in those studies could be explained by the use of different starting samples, pressure transmitting medium and/or pressure calibrant. First of all, the SiO_2 glasses samples used in those studies were obtained from different synthesis methods (e.g., quenching rates) and therefore have different initial local structures and properties (Murakami & Bass, 2010; Sun et al., 2022; Zha et al., 1994). In particular, the starting sample used in Zha et al. (1994) was Herasil type II SiO_2 glass with a density of 2.20 g/cm^3, a V_S of 3.89 km/s, and a V_P of 6.20 km/s at ambient conditions. The starting sample of SiO_2 glass in Murakami and Bass (2010) was Suprasil-P SiO_2 glass with a V_S of ~3.66 km/s at ambient conditions. The starting sample of SiO_2 glass in Sun et al. (2022) was produced by burning $SiCl_4$ with O_2 at 2,100°C, and its density, V_S and V_P at ambient pressure are 2.11 g/cm^3, 3.90 km/s and 6.14 km/s, respectively. The starting density and V_S of these silica glasses differ by approximately 7%, reflecting their local structural differences. In addition, helium and neon could more easily enter the silica structure whereas the methanol-ethanol (M-E) mixture would not (H. Yang et al., 2021). At high pressure, the sound velocity of SiO_2 glass in the pressure-transmitting medium of helium is higher than that in the pressure-transmitting medium of the M-E mixture (Figure S3 in Supporting Information S1). Furthermore, pressure determinations can be influenced by the use of different pressure calibrants such as ruby versus metals (Au and Pt). In summary, the difference in the synthesis method, pressure transmitting medium and pressure calibrant between amorphous glasses could generate certain uncertainties in their high-pressure sound velocities.

3.5. Shear Wave Velocity Trend of Silicate Glass at 45–63 GPa

The V_S–P profile of our basaltic glass exhibits a nearly linear trend at 38–63 GPa, a feature also observed in another basaltic glass above 45 GPa (Trubowitz et al., 2024). Within this pressure range of 45–63 GPa, the coordination numbers of Mg-O, Al-O, and Fe-O are expected to increase gradually, whereas the Ca-O coordination number remains nearly constant with increasing pressure (Bajgain et al., 2015; Karki et al., 2018; Majumdar et al., 2020; Solomatova & Caracas, 2019). Such variations in cation coordination numbers may influence the evolution of V_S in chemically complex silicate glasses. The comparable *dVs/dP* values of two basaltic glasses suggest that the notable discrepancy in MgO content (~14 mol.%) does not produce a visible change in structural compressibility at 45–63 GPa (Figure 4 and Table S2 in Supporting Information S1). Additionally, basaltic glasses exhibit a flatter V_S–P trend than pyrolitic glass at 45–63 GPa (Figure 4) (Huang et al., 2022; Trubowitz et al., 2024). As illustrated in Table S2 in Supporting Information S1, our basaltic glass contains ~6 mol.% more Al_2O_3 and ~22 mol.% lower MgO than pyrolitic glass. Similarly, another basaltic glass composition shows ~36 mol.% lower MgO and ~6 mol.% more Al_2O_3 relative to pyrolitic glass (Huang et al., 2022; Trubowitz et al., 2024). The FeO content between pyrolytic glass and the two basaltic glasses is comparable (~6 mol.%). Therefore, the ~6 mol.% difference in Al_2O_3 content maybe the cause for the small divergence in the V_S profiles between basaltic and pyrolitic glass samples, which is also reported in Trubowitz et al. (2024).

4. Geophysical Implications

The most significant result in this study is the combined V_P and V_S data and Poisson's ratio trends of the basaltic glass at 25–63 GPa, which have not been previously explored for silicate glasses. In addition, comparison with previous data reveals that Al_2O_3 can enhance the V_S and V_P of basaltic glasses, whereas FeO and CaO both tend to decrease these velocities. From these data, we observe that the Al_2O_3 and FeO exert opposing effects on the sound velocities of basaltic glasses, and the increase in Al_2O_3 content leads to a slight reduction in the compressibility of basaltic glasses at 45–63 GPa.

The compositional effects of basaltic glass may serve as an analog for inferring properties of basaltic melts (Morard et al., 2020). Accordingly, our results suggest that the elasticity of basaltic melts is significantly affected by the partitioning of Al and Fe between co-existing basaltic melts and crystals in the lower mantle. Taking into account the affinity of iron and aluminum for melts, basaltic melts at Earth's lower-mantle pressures are estimated to contain approximately 13–30 mol.% Al_2O_3 and 15–22 mol.% FeO (Andrault et al., 2012; Nomura et al., 2011). The compressibility of basaltic glass could be further reduced by the 13–30 mol.% Al_2O_3 addition, whereas the effect of 15–22 mol.% FeO on the compressibility of basaltic glass remains unclear. The increase in sound velocities of basaltic melts induced by 13–30 mol.% Al_2O_3 may be mitigated by the coexistence of 15–22 mol.% FeO at mid-lower mantle depths (~1,500 km), making it less visible seismically. Basaltic melts with significant amounts of FeO and Al_2O_3 may also become less buoyant (with less density contrast) at the mid-lower mantle depth of 1,500 km.

Data Availability Statement

Data sets for the high-pressure experimental measurements are available at Su (2023).

Acknowledgments
This work is supported by the National Natural Science Foundation of China (42404117 and 42072052). J.F. Lin acknowledges supports from the U.S. National Science Foundation (EAR-2333879).

References

Andrault, D., Petitgirard, S., Lo Nigro, G., Devidal, J. L., Veronesi, G., Garbarino, G., & Mezouar, M. (2012). Solid-liquid iron partitioning in Earth's deep mantle. *Nature*, *487*(7407), 354–357. https://doi.org/10.1038/nature11294

Aoki, K., Sakamaki, T., Ohashi, T., Ikeda, O., & Suzuki, A. (2020). Effects of alkali and alkaline-earth cations on the high-pressure sound velocities of aluminosilicate glasses. *Physics and Chemistry of Minerals*, *47*(6), 28. https://doi.org/10.1007/s00269-020-01098-3

Bajgain, S., Ghosh, D. B., & Karki, B. B. (2015). Structure and density of basaltic melts at mantle conditions from first-principles simulation. *Nature Communications*, *6*(1), 8578. https://doi.org/10.1038/ncomms9578

Benmore, C. J., Soignard, E., Amin, S. A., Guthrie, M., Shastri, S. D., Lee, P. L., & Yarger, J. L. (2010). Structural and topological changes in silica glass at pressure. *Physical Review B*, *81*(5), 054105. https://doi.org/10.1103/PhysRevB.81.054105

Clark, A. N., Lesher, C. E., Jacobsen, S. D., & Wang, Y. (2016). Anomalous density and elastic properties of basalt at high pressure: Reevaluating of the effect of melt fraction on seismic velocity in the Earth's crust and upper mantle. *Journal of Geophysical Research: Solid Earth*, *121*(6), 4232–4248. https://doi.org/10.1002/2016JB012973

Dauphas, N., Roskosz, M., Alp, E. E., Neuville, D. R., Hu, M. Y., Sio, C. K., et al. (2014). Magma redox and structural controls on iron isotope variations in Earth's mantle and crust. *Earth and Planetary Science Letters*, *398*, 127–140. https://doi.org/10.1016/j.epsl.2014.04.033

Du, Z., Deng, J., Miyazaki, Y., Mao, H. K., Karki, B. B., & Lee, K. K. (2019). Fate of hydrous Fe-rich silicate melt in Earth's deep mantle. *Geophysical Research Letters*, *46*(16), 9466–9473. https://doi.org/10.1029/2019GL083633

Dufils, T., Folliet, N., Mantisi, B., Sator, N., & Guillot, B. (2017). Properties of magmatic liquids by molecular dynamics simulation: The example of a MORB melt. *Chemical Geology*, *461*, 34–46. https://doi.org/10.1016/j.chemgeo.2016.06.030

Elliott, S. R. (1992). The origin of the first sharp diffraction peak in the structure factor of covalent glasses and liquids. *Journal of Physics: Condensed Matter*, *4*(38), 7661–7678. https://doi.org/10.1088/0953-8984/4/38/003

Feng, S., Majumdar, A., Kuang, H., Pan, Y., Iitaka, T., & Tse, J. S. (2021). A comparative study on pressure-induced structural transformations in a basaltic glass and melt from ab initio molecular dynamics calculations. *Physics and Chemistry of Minerals*, *48*(11), 41. https://doi.org/10.1007/s00269-021-01165-3

Fu, S., Yang, J., Zhang, Y., Liu, J., Greenberg, E., Prakapenka, V. B., et al. (2018). Melting behavior of the lower-mantle ferropericlase across the spin crossover: Implication for the ultra-low velocity zones at the lowermost mantle. *Earth and Planetary Science Letters*, *503*, 1–9. https://doi.org/10.1016/j.epsl.2018.09.014

Fu, S. Y., Yang, J., & Lin, J. F. (2017). Abnormal elasticity of single-crystal magnesiosiderite across the spin transition in Earth's lower mantle. *Physical Review Letters*, *118*(3), 036402. https://doi.org/10.1103/PhysRevLett.118.036402

Geballe, Z. M., Arveson, S. M., Speziale, S., & Jeanloz, R. (2022). Sound speed and refractive index of amorphous $CaSiO_3$ upon pressure cycling to 40 GPa. *American Mineralogist*, *107*(12), 2212–2218. https://doi.org/10.2138/am-2022-8081

Ghosh, D. B., Karki, B. B., & Stixrude, L. (2014). First-principles molecular dynamics simulations of $MgSiO_3$ glass: Structure, density, and elasticity at high pressure. *American Mineralogist*, *99*(7), 1304–1314. https://doi.org/10.2138/am.2014.4631

Gu, J. T., Fu, S., Gardner, J. E., Yamashita, S., Okuchi, T., & Lin, J. F. (2021). Nonlinear effects of hydration on high-pressure sound velocities of rhyolitic glasses. *American Mineralogist: Journal of Earth and Planetary Materials*, *106*(7), 1143–1152. https://doi.org/10.2138/am-2021-7597

Hemley, R. J., Mao, H. K., Bell, P. M., & Mysen, B. O. (1986). Raman spectroscopy of SiO_2 glass at high pressure. *Physical Review Letters*, *57*(6), 747–750. https://doi.org/10.1103/PhysRevLett.57.747

Hennet, L., Pozdnyakova, I., Cristiglio, V., Cuello, G. J., Jahn, S., Krishnan, S., et al. (2007). Short- and intermediate-range order in levitated liquid aluminates. *Journal of Physics: Condensed Matter*, *19*(45), 455210. https://doi.org/10.1088/0953-8984/19/45/455210

Huang, D., Murakami, M., Bodholt, J., McCammon, C., & Petitgirard, S. (2022). Structural evolution in a pyrolitic magma ocean under mantle conditions. *Earth and Planetary Science Letters*, *584*, 117473. https://doi.org/10.1016/j.epsl.2022.117473

Karki, B. B., Ghosh, D. B., & Bajgain, S. K. (2018). Simulation of silicate melts under pressure. *Magmas Under Pressure*, 419–453. https://doi.org/10.1016/b978-0-12-811301-1.00016-2

Kono, Y., Ohara, K., Kondo, N. M., Yamada, H., Hiroi, S., Noritake, F., et al. (2022). Experimental evidence of tetrahedral symmetry breaking in SiO_2 glass under pressure. *Nature Communications*, *13*(1), 2292. https://doi.org/10.1038/s41467-022-30028-w

Kono, Y., Shibazaki, Y., Benson, C. K., Wang, Y., & Shen, G. (2018). Pressure-induced structural change in $MgSiO_3$ glass at pressures near the Earth's core-mantle boundary. *Proceedings of the National Academy of Sciences*, *115*(8), 1742–1747. https://doi.org/10.1073/pnas.1716748115

Labrosse, S., Hernlund, J. W., & Coltice, N. (2007). A crystallizing dense magma ocean at the base of the Earth's mantle. *Nature*, *450*(7171), 866–869. https://doi.org/10.1038/nature06355

Lee, S. K., Kim, Y. H., Yi, Y. S., Chow, P., Xiao, Y., Ji, C., & Shen, G. (2019). Oxygen Quadclusters in SiO_2 glass above megabar pressures up to 160 GPa revealed by X-ray Raman scattering. *Physical Review Letters*, *123*(23), 235701. https://doi.org/10.1103/physrevlett.123.235701

Lee, S. K., Lin, J. F., Cai, Y. Q., Hiraoka, N., Eng, P. J., Okuchi, T., et al. (2008). X-ray Raman scattering study of $MgSiO_3$ glass at high pressure: Implication for triclustered $MgSiO_3$ melt in Earth's mantle. *Proceedings of the National Academy of Sciences*, *105*(23), 7925–7929. https://doi.org/10.1073/pnas.0802667105

Lin, J. F., Fukai, H., Prendergast, D., Okuchi, T., Cai, Y. Q., Hiraoka, N., et al. (2007). Electronic bonding transition in compressed SiO_2 glass. *Physical Review B*, *75*(1), 012201. https://doi.org/10.1103/PhysRevB.75.012201

Liu, J., Dauphas, N., Roskosz, M., Hu, M. Y., Yang, H., Bi, W., et al. (2017). Iron isotopic fractionation between silicate mantle and metallic core at high pressure. *Nature Communications*, *8*(1), 14377. https://doi.org/10.1038/ncomms14377

Liu, J., & Lin, J. F. (2014). Abnormal acoustic wave velocities in basaltic and (Fe,Al)-bearing silicate glasses at high pressures. *Geophysical Research Letters*, *41*(24), 8832–8839. https://doi.org/10.1002/2014gl062053

Lobanov, S. S., Speziale, S., Winkler, B., Milman, V., Refson, K., & Schifferle, L. (2022). Electronic, structural, and mechanical properties of SiO_2 glass at high pressure inferred from its refractive index. *Physical Review Letters*, *128*(7), 077403. https://doi.org/10.1103/PhysRevLett.128.077403

Majumdar, A., Wu, M., Pan, Y., Iitaka, T., & Tse, J. S. (2020). Structural dynamics of basaltic melt at mantle conditions with implications for magma oceans and superplumes. *Nature Communications*, *11*(1), 4815. https://doi.org/10.1038/s41467-020-18660-w

Mao, H. K., Xu, J., & Bell, P. M. (1986). Calibration of the ruby pressure gauge to 800 kbar under quasi-hydrostatic conditions. *Journal of Geophysical Research*, *91*(B5), 4673–4676. https://doi.org/10.1029/JB091iB05p04673

Mashino, I., Murakami, M., Kitao, S., Mitsui, T., Masuda, R., & Seto, M. (2022). Acoustic wave velocities of ferrous-bearing $MgSiO_3$ glass up to 158 GPa with implications for dense silicate melts at the base of the Earth's mantle. *Geophysical Research Letters*, *49*(19), e2022GL098279. https://doi.org/10.1029/2022GL098279

Meade, C., Hemley, R. J., & Mao, H. K. (1992). High-pressure X-ray diffraction of SiO_2 glass. *Physical Review Letters*, *69*(9), 1387–1390. https://doi.org/10.1103/PhysRevLett.69.1387

Morard, G., Hernandez, J., Guarguaglini, M., Bolis, R., Benuzzi-mounaix, A., Vinci, T., et al. (2020). In situ X-ray diffraction of silicate liquids and glass under dynamic and static compression to megabar pressures. *Proceedings of the National Academy of Sciences*, *117*(22), 1–6. https://doi.org/10.1073/pnas.1920470117

Murakami, M., & Bass, J. D. (2010). Spectroscopic evidence for ultrahigh-pressure polymorphism in SiO_2 glass. *Physical Review Letters*, *104*(2), 025504. https://doi.org/10.1103/PhysRevLett.104.025504

Murakami, M., & Bass, J. D. (2011). Evidence of denser $MgSiO_3$ glass above 133 gigapascal (GPa) and implications for remnants of ultradense silicate melt from a deep magma ocean. *Proceedings of the National Academy of Sciences*, *108*(42), 17286–17289. https://doi.org/10.1073/pnas.1109748108

Nomura, R., Ozawa, H., Tateno, S., Hirose, K., Hernlund, J., Muto, S., et al. (2011). Spin crossover and iron-rich silicate melt in the Earth's deep mantle. *Mineralogical Magazine*, *473*(7346), 199–202. https://doi.org/10.1038/nature09940

Ohira, I., Murakami, M., Kohara, S., Ohara, K., & Ohtani, E. (2016). Ultrahigh-pressure acoustic wave velocities of SiO_2-Al_2O_3 glasses up to 200 GPa. *Progress in Earth and Planetary Science*, *3*(1), 18. https://doi.org/10.1186/s40645-016-0097-2

Ohtani, E., & Maeda, M. (2001). Density of basaltic melt at high pressure and stability of the melt at the base of the lower mantle. *Earth and Planetary Science Letters*, *193*(1–2), 69–75. https://doi.org/10.1016/S0012-821X(01)00505-2

Ohtani, E., Nagata, Y., Suzuki, A., & Kato, T. (1995). Melting relations of peridotite and the density crossover in planetary mantles. *Chemical Geology*, *120*(3–4), 207–221. https://doi.org/10.1016/0009-2541(94)00139-Y

Petitgirard, S., Malfait, W. J., Journaux, B., Collings, I. E., Jennings, E. S., Blanchard, I., et al. (2017). SiO_2 glass density to lower-mantle pressures. *Physical Review Letters*, *119*(21), 215701. https://doi.org/10.1103/PhysRevLett.119.215701

Petitgirard, S., Malfait, W. J., Sinmyo, R., Kupenko, I., Hennet, L., Harries, D., et al. (2015). Fate of $MgSiO_3$ melts at core-mantle boundary conditions. *Proceedings of the National Academy of Sciences*, *112*(46), 14186–14190. https://doi.org/10.1073/pnas.1512386112

Prescher, C., Parkapenka, V. B., Stefansji, J., Jahn, S., Skinner, L. B., & Wang, Y. (2017). Beyond sixfold coordinated Si in SiO_2 glass at ultrahigh pressures, *114*(38), 10041–10046. https://doi.org/10.1073/pnas.1708882114

Price, D. L., Moss, S. C., Reijers, R., Saboungi, M. L., & Susman, S. (1988). Intermediate-range order in glasses and liquids. *Journal of Physics: Condensed Matter*, *1*(5), 1005–1008. https://doi.org/10.1088/0953-8984/1/5/017

Saha, P., Murakami, M., McCammon, C., Liebske, C., & Krymarys, E. (2023). Ultrahigh-pressure acoustic velocities of aluminous silicate glass up to 155 GPa with implications for the structure and dynamics of the deep terrestrial magma ocean. *Geophysical Research Letters*, *50*(14), e2023GL103614. https://doi.org/10.1029/2023GL103614

Sakamaki, T., Kono, Y., Wang, Y., Park, C., Yu, T., Jing, Z., & Shen, G. (2014). Contrasting sound velocity and intermediate-range structural order between polymerized and depolymerized silicate glasses under pressure. *Earth and Planetary Science Letters*, *391*, 288–295. https://doi.org/10.1016/j.epsl.2014.02.008

Sanchez-Valle, C., & Bass, J. D. (2010). Elasticity and pressure-induced structural changes in vitreous $MgSiO_3$-enstatite to lower mantle pressures. *Earth and Planetary Science Letters*, *295*(3–4), 523–530. https://doi.org/10.1016/j.epsl.2010.04.034

Sato, T., & Funamori, N. (2008). Sixfold-coordinated amorphous polymorph of SiO_2 under high pressure. *Physical Review Letters*, *101*(25), 255502. https://doi.org/10.1103/PhysRevLett.101.255502

Sato, T., & Funamori, N. (2010). High-pressure structural transformation of SiO_2 glass up to 100 GPa. *Physical Review B*, *82*, 184102. https://doi.org/10.1103/PhysRevB.82.184102.82(18)

Shim, S. H., & Catalli, K. (2009). Compositional dependence of structural transition pressures in amorphous phases with mantle-related compositions. *Earth and Planetary Science Letters*, *283*(1–4), 174–180. https://doi.org/10.1016/j.epsl.2009.04.018

Shimoda, K., & Okuno, M. (2006). Molecular dynamics study of $CaSiO_3$-$MgSiO_3$ glasses under high pressure. *Journal of Physics: Condensed Matter*, *18*(28), 6531–6544. https://doi.org/10.1088/0953-8984/18/28/008

Solomatova, N. V., & Caracas, R. (2019). Pressure-induced coordination changes in a pyrolitic silicate melt from ab initio molecular dynamics simulations. *Journal of Geophysical Research: Solid Earth*, *124*(11), 11323–11350. https://doi.org/10.1029/2019JB018238

Stixrude, L., & Bukowinski, M. S. T. (1991). Atomic-structure of SiO_2 glass and its response to pressure. *Physical Review B*, *44*(6), 2523–2534. https://doi.org/10.1103/PhysRevB.44.2523

Su, X. (2023). Sound velocities of basaltic glass at Earth's deep-mantle pressures. *Zenodo*. https://doi.org/10.5281/zenodo.7916793

Sun, N. Y., Mao, Z., Zhang, X. Y., Tkachev, S. N., & Lin, J. F. (2022). Hot dense silica glass with ultrahigh elastic moduli. *Scientific Reports*, *12*(1), 13946. https://doi.org/10.1038/s41598-022-18062-6

Susman, S., Volin, K. J., Montague, D. G., & Price, D. L. (1990). The structure of vitreous and liquid GeS_2: A neutron diffraction study. *Journal of Non-Crystalline Solids*, *125*, 168180. https://doi.org/10.1016/0022-3093(90)90336-K

Trubowitz, C., Murakami, M., Petitgirard, S., Liebske, C., & McCammon, C. (2024). Structural evolution of basaltic melts in the deep Earth: Insights from high-pressure sound velocity. *Journal of Geophysical Research: Solid Earth*, *129*, e224JB028969. https://doi.org/10.1029/2024JB028969

Wei, X., Dong, L., Li, F., Zhou, Q., Guo, M., Wei, Y., et al. (2022). Effect of Al_2O_3 on sound velocity of $MgSiO_3$ glass at high pressure. *Minerals*, *12*(9), 1069. https://doi.org/10.3390/min12091069

Williams, Q., & Jeanloz, R. (1988). Spectroscopic evidence for pressure-induced coordination changes in silicate glasses and melts. *Science*, *239*(4842), 902–905. https://doi.org/10.1126/science.239.4842.902

Xu, M., Jing, Z., Chantel, J., Jiang, P., Yu, T., & Wang, Y. (2018). Ultrasonic velocity of diopside liquid at high pressure and temperature: Constraints on velocity reduction in the upper mantle due to partial melts. *Journal of Geophysical Research: Solid Earth*, *123*(10), 8676–8690. https://doi.org/10.1029/2018jb016187

Yang, H., Gleason, A. E., Tkachev, S. N., Chen, B., Jeanloz, R., & Mao, W. L. (2021). Noble incorporation into silicate glasses: Implications for planetary volatile storage. *Geochemical Perspectives Letter*, *17*, 1–5. https://doi.org/10.7185/geochemlet.2105

Yang, J., Lin, J. F., Jacobsen, S. D., Seymour, N. M., Tkachev, S. N., & Prekapenka, V. B. (2016). Elasticity of ferropericlase and seismic heterogeneity in the Earth's lower mantle. *Journal of Geophysical Research: Solid Earth*, *121*(12), 8488–8500. https://doi.org/10.1002/2016JB013352

Yang, J., Mao, Z., Lin, J. F., & Prakapenka, V. B. (2014). Single-crystal elasticity of the deep-mantle magnesite at high pressure and temperature. *Earth and Planetary Science Letters*, *392*, 292–299. https://doi.org/10.1016/j.epsl.2014.01.027

Yang, J., Tong, X., Lin, J. F., Okuchi, T., & Tomioka, N. (2015). Elasticity of ferropericlase across the spin crossover in the Earth's lower mantle. *Scientific Reports*, *5*(1), 1–9. https://doi.org/10.1038/srep17188

Zha, C. S., Hemley, R. J., Mao, H. K., Duffy, T. S., & Meade, C. (1994). Acoustic velocities and refractive index of SiO_2 glass to 57.5 GPa by Brillouin scattering. *Physical Review B*, *50*(18), 13105–13112. https://doi.org/10.1103/PhysRevB.50.13105

References From the Supporting Information

Coasne, B., Weigel, C., Polian, A., Kint, M., Rouquette, J., Haines, J., et al. (2014). Poroelastic theory applied to the adsorption-induced deformation of vitreous silica. *The Journal of Physical Chemistry B*, *118*(49), 14519–14525. https://doi.org/10.1021/jp5094383

Weigel, C., Polian, A., Kint, M., Ruffle, B., Foret, M., & Vacher, R. (2012). Vitreous silica distends in helium gas: Acoustic versus static compressibilities. *Physical Review Letters*, *109*(24), 245504. https://doi.org/10.1103/PhysRevLett.109.245504